Significant triboelectric enhancement using interfacial piezoelectric ZnO nanosheet layer

Narasimulu, A. A., Zhao, P., Soin, N., Prashanthi, K., Ding, P., Chen, J., Dong, S., Chen, L., Zhou, E., Montemagno, C. D., & Luo, J. (2017). Significant triboelectric enhancement using interfacial piezoelectric ZnO nanosheet layer. *Nano Energy*, *40*, 471-480. https://doi.org/10.1016/j.nanoen.2017.08.053

Link to publication record in Ulster University Research Portal

Published in:
Nano Energy

Publication Status:
Published (in print/issue): 31/10/2017

DOI:
10.1016/j.nanoen.2017.08.053

Document Version
Author Accepted version

General rights
Copyright for the publications made accessible via Ulster University's Research Portal is retained by the author(s) and / or other copyright owners and it is a condition of accessing these publications that users recognise and abide by the legal requirements associated with these rights.

Take down policy
The Research Portal is Ulster University's institutional repository that provides access to Ulster's research outputs. Every effort has been made to ensure that content in the Research Portal does not infringe any person's rights, or applicable UK laws. If you discover content in the Research Portal that you believe breaches copyright or violates any law, please contact pure-support@ulster.ac.uk.

Download date: 04/05/2023

Significant triboelectric enhancement using interfacial piezoelectric ZnO nanosheet layer

Anand A. Narasimulu,[a,†] Pengfei Zhao,[a,†] Navneet Soin,[a,†] Kovur Prashanthi,[b] Peng Ding, [c] Jinkai Chen,[c] Shurong Dong,[c] Li Chen[d], Erping Zhou[a], Carlo D Montemagno[b], and Jikui Luo[a]*

[a]Institute for Materials Research and Innovation (IMRI), University of Bolton, Deane Road, Bolton, BL3 5AB, United Kingdom

[b]Ingenuity Lab, Department of Chemical and Materials Engineering, University of Alberta, Edmonton, Alberta, T6G 2V4, Canada

[c]Department of Information Science & Electrical Engineering, Zhejiang University, 38 Zheda Road, Hangzhou 310027, P. R. China

[d]Faculty of Engineering, University of Leeds, Woodhouse Lane, Leeds, LS2 9JT, United Kingdom

†These authors contributed equally to the work.

*Corresponding Author: Jikui Luo,

Institute for Materials Research and Innovation (IMRI),

The University of Bolton,

Deane Road, Bolton,

BL3 5AB, United Kingdom

Email: j.luo@bolton.ac.uk

Abstract:

Utilising an interfacial piezoelectric ZnO nanosheet layer, a significant enhancement in the power density is reported for the triboelectric nanogenerators (TENG) based on phase inversion membranes of polyvinylidene fluoride (PVDF) and polyamide-6 (PA6). At an applied force of 80 N, the TENG device incorporating electrochemically deposited ZnO nanosheets produces an output voltage of ~625 V and a current density of ~40 mAm^{-2} (corresponding a charge density of 100.6 μCm^{-2}), respectively; significantly higher than ~310 V and ~10 mAm^{-2} (corresponding a charge density of 77.45 μCm^{-2}) for the pristine TENG device. The enhancement in the surface charge density provided by the interfacial piezoelectric ZnO layer is also reflected in the high piezoelectric coefficient d_{33} (-74 pmV^{-1}) as compared to the pristine fluoropolymer membranes (-50 pmV^{-1}). For tribo-negative membranes incorporating the interfacial ZnO layer, piezoelectric force microscopy measurements further show enhanced domain size which can be attributed to the interfacial dipole-dipole interaction with the ferroelectric polarization of PVDF, which promotes the alignment with the polar axis of ZnO. Under compressive stress, the piezoelectric potential thus produced in the ZnO nanosheets provides charge injection on to the surface of $ZnSnO_3$-PVDF membrane, improving the charge density, which in-turn significantly enhances the power density from 0.11 to ~1.8 W/m^2. The TENG devices thus fabricated using a facile electrochemical deposition and phase inversion technique show enhanced output power without the need for high electric field poling or external charge injection process by relying on coupling of triboelectric and piezoelectric effects.

1. Introduction

Significant development in technologies has made electronic systems smaller, faster, portable and highly energy efficient [1]. Since the typical power consumption for such electronic systems is very low, it is feasible to power these electronic systems with batteries or portable power sources. Recently, emphasis is being placed on advancing the existing energy harvesting techniques to realise self-powered and battery-free systems [1]. To this

effect, various micro-energy sources and storage architectures have been developed such as fuel cells, photovoltaic cells, super capacitors, piezoelectric nanogenerators (PENG) and more recently, triboelectric nanogenerators (TENG) [3, 4]. The TENG devices have gained special attention for self-powered electronics and remote sensing network applications owing to their unique advantages, including simple device fabrication, cost effective materials, high efficiency and large output power [5, 6].

The principle of TENGs is to utilise charges that are generated on the surfaces of two dissimilar materials in contact through electrification and electrostatic effects. It is believed that chemical bonds are formed between some parts of the two surfaces of the materials in contact by moving charges to equalise the electrochemical potential. When separated, some of the bonded atoms either give away electrons or gain extra electrons, which produce triboelectric charges on the surface of the materials. When two dissimilar dielectric materials carrying opposite triboelectric charges make a relative motion, an electric potential difference is produced. This electric potential difference moves charges through the conductive back metal electrodes of the TENG and external circuit, thus powering the connected device or system [1, 5]. Current efforts for enhancing the conversion efficiency and output performance of TEG [6, 7] mainly focus on the enhancement in the triboelectric charge density (σ) *via* the following methods: (i) judicious selection of suitable triboelectric materials with large difference in their triboelectric polarities; (ii) enhancement of the effective contact area of the triboelectric materials by surface functionalisation [7], silicon template based micro/nanopatterning [1, 9], introduction of inorganic/organic nanostructures [4] and finally, (iii) enhancement of charge density *via* charge injection/polarisation by addition of piezoelectric additives and production of hybrid piezoelectric/triboelectric structures [9]. The simulation analysis carried out for enhanced power output observed for the combined piezoelectric, triboelectric systems has revealed the following coupling types:

(i) addition of electrostatic charges directly onto the piezoelectric material surface through contact with another material to enhance the piezoelectric potential difference [10];

(ii) by utilising a single common electrode between triboelectric and piezoelectric parts of the device, thus adding the triboelectric charges onto the piezoelectric electrode and improving the power output [12, 13];

(iii) through rational structure design, developing a single device structure capable of generating both piezoelectric and triboelectric outputs in a single press and release cycle [14, 15].

Polyvinylidene fluoride (PVDF), owing to the presence of strong electronegative fluorine groups, is an excellent choice for introducing simultaneous piezoelectric and triboelectric effects. The material not only demonstrates strong negative triboelectric properties, but also displays polarisation effect which increases the triboelectric charge density on the surface as demonstrated by a number of previous works [6, 15], including ours [16]. The polar β-phase PVDF forms a planar zigzag (TTT) structure which creates an organised crystal, allowing a higher packing density with the alignment of the charged fluorine atoms producing a net polarisation [16]. Thus, the use of PVDF with high crystallinity and β-phase content could further improve the performance of the TENGs as demonstrated by our previous work [16]. Zinc oxide (ZnO) is a unique semiconducting, piezoelectric material with diverse nanostructured morphologies and has recently attained substantial interests for the fabrication of energy harvesting devices [3, 18, 19]. Owing to its simple and low-temperature growth techniques, facile growth conditions, strong orientation effects, excellent flexibility and bio-compatibility, ZnO nanostructures have been utilised widely for PENG and TENG applications [3, 4, 6, 19-21]. Unlike PVDF, whose piezoelectric properties arise due to the presence of polar β-phase, the piezoelectric properties of ZnO nanostructures are attributed to the coupling of its piezoelectric and semiconductor properties. The incorporation of ZnO nanostructures was found to have a significant effect on enhancing the performance of TENGs *via* a combination of triboelectric and piezoelectric effects [4]. In our earlier work, we have reported on the enhancement of power output of TENGs *via* the incorporation of piezoelectric zinc stannate ($ZnSnO_3$) in dielectric PVDF matrix [15]. However, it is known that the mixing of high surface area nanomaterials is inherently difficult in a high viscosity polymer melt, and as such the random distribution and orientation of resulting ZnO, $ZnSnO_3$ nanomaterials can potentially hamper the polarisation induced charge density. On the other hand, ZnO nanomaterials grown on a substrate with aligned (0002) crystal orientation along the contact force direction are expected to have a better effect on the performance of TENGs.

Here, we report on the significant effect of utilising an interfacial layer consisting of well aligned piezoelectric ZnO nanosheets for enhancing the power output of PVDF/PA6 based TENGs with an aluminium (Al) substrate acting both as the substrate for the seedless growth of ZnO nanosheets and as the charge collector electrode. Further deposition of fluoropolymer

membranes comprising of PVDF or $ZnSnO_3$-PVDF by phase-inversion technique on these ZnO/Al substrates provides the triboelectric negative substrates. The phase-inversion polyamide (PA6) membrane provides the judicious triboelectric positive substrate, thus completing the face-to-face configuration of the vertical contact-mode TENG. Our results show that the use of well-aligned ZnO nanosheets as the interfacial piezoelectric layer can significantly improve the charge and power density with values of up to 100.6 $\mu C/m^2$ and ~1.8 W/m^2, as compared to 77.4 $\mu C/m^2$ and ~0.11 W/m^2 for pristine samples without the interfacial ZnO, respectively. This enhancement is mainly attributed to the high charge density induced by the polarisation of ZnO nanosheets under the compressive force.

2. Experimental

2.1 Materials

As discussed earlier, the TENG consists of materials with opposite triboelectric polarities. By observing the triboelectric series, it can be observed that polyamide tends to lose electrons, while fluoropolymers such as PVDF have a strong ability to gain electrons, and thus the PVDF/PA6 combination represents a judicious selection of materials. In this work, the PA6 membrane was used as the positive side material, and PVDF or PDVF incorporated with $ZnSnO_3$ nanomaterial ($ZnSnO_3$-PVDF in short hereafter) on ZnO nanosheets was used as the negative side material to fabricate TENGs, as shown in Fig. 1.

Polyamide-6 (PA6, TECHNYL 1011R) was obtained from Rhodia Polymers Ltd,; PVDF (SOLEF 1006) from Solvay Solxeis Ltd. and $ZnSnO_3$ nanocube powders (Flamtard S, approximate size 400-500 nm) were obtained from William Blythe Ltd (U.K.), respectively. Aluminium sheet, zinc nitrate hexahydrate $Zn(NO_3)_2 \cdot 6H_2O$ (99.9% purity) and Hexamethylenetetramine (HMTA) (99.9% purity) were purchased from Sigma-Aldrich. For the preparation of 5 wt% $ZnSnO_3$-PVDF composites, the samples were prepared using high-speed twin screw compounding process. The complete details of the compounding process including the temperature profile and screw speeds can be found in our earlier work [15].

2.2 Electrochemical deposition of ZnO nanosheets

The ZnO nanosheets were synthesised *via* a facile electrochemical deposition (ED) technique using a CHI601D potentiostat (CHI 601D, CH Instruments, USA) and a homemade electrochemical cell utilising a three-electrode setup. For the ED process, a 0.5 mm thick Al

foil, Pt wire and a saturated calomel electrode (SCE) were used as the working, counter and reference electrode, respectively. Prior to the ED process, the Al working electrode (2 cm x 2 cm) was first cleaned in an ultrasonic bath for approximately 5 min each with acetone, isopropanol and deionised (DI) water, respectively. The electrolyte solution with pH ~5.7 was prepared by dissolving equimolar concentration of 0.025 M zinc nitrate hexahydrate ($Zn(NO_3)_2 \cdot 6H_2O$) and hexamethylenetetramine (HMTA) in DI water. For the growth of ZnO nanosheets, a potential of -0.7 V was applied between the electrodes, while the temperature of the electrolyte solution was maintained at 70 °C. The precursor solution was stirred continuously for the whole duration of the deposition (3 hrs) to achieve high uniformity of the deposited nanomaterials. After the growth process, the as-prepared ZnO/Al substrates were rinsed with DI water to remove any residual salts and further dried at room temperature for the subsequent deposition of PVDF or PVDF-$ZnSnO_3$ films.

2.3 Membrane preparation by phase-inversion process

The deposition of PVDF, $ZnSnO_3$-PVDF and PA6 films was carried out in accordance with our previous studies [16, 22]. Briefly, the solutions for the synthesis of the membranes were prepared using a 20 wt% dope solution in the corresponding solvents (Formic acid for PA6 and *N, N*-Dimethlyformamide (DMF) for PVDF, respectively) by continuously stirring the polymer pellets and solvents at ~70 ^{o}C for 3 hrs [15]. After preparation of the dope solution, a certain volume of the PVDF or $ZnSnO_3$-PVDF solution was deposited on the electrochemically deposited ZnO/Al substrate *via* a spin-coating (Spin 150 processor) process using the following protocol: initial spinning at 500 rpm for 10 sec, followed by 2000 rpm for 30 sec. The thus obtained PVDF or $ZnSnO_3$-PVDF coated ZnO/Al substrates were then immersed immediately in an anti-solvent bath (DI water) kept at a desired quenching temperature of ~5°C. The resulting PVDF/ZnO/Al or $ZnSnO_3$-PVDF/ZnO/Al substrates were then rinsed repeatedly with DI water to remove any residual solvent and dried at room temperature for further assembling of the triboelectric generators. The preparation of free-standing PA6 membranes was carried out in accordance with our previous studies [15].

2.4 Fabrication of triboelectric generators

The as-prepared PA6 membrane was attached *via* an adhesive aluminium conductive tape electrode to an acrylic sheet. For the bottom part of the TENG, various combinations of

ZnO/Al, PVDF/ZnO/Al and $ZnSnO_3$-PVDF/ZnO/Al were assembled, as shown in Fig. 1 and summarised in Table 1. Sample S1 consists of a ZnO nanosheet layer grown on an aluminium substrate; S2 has a PVDF/ZnO/Al structure, while S4 has a 5wt% $ZnSnO_3$-PVDF/ZnO/Al structure. Sample S3 (5wt% $ZnSnO_3$-PVDF/Al) has the same structure as that of S4, but without the interfacial ZnO nanosheet layer. All the TENG devices have dimensions of 2 cm x 2 cm with a small extension of the acrylic sheet for connecting leads. Two arc-shaped polyimide sheets were used to maintain the desired spacing between the top and bottom parts of the TENG, as shown in Fig. 1.

2.5 Material characterisation and electrical testing

The surface and cross-sectional morphology of the samples were analysed using a Hitachi S-3400N scanning electron microscope (SEM) equipped with an Oxford Instruments INCA EDS system. The vibrational characteristics of the polymeric films were examined using Fourier transform infrared spectroscopy (FTIR, Thermo Scientific IS10 Nicolet). The spectra were recorded at a nominal resolution of ±1 cm^{-1} for a total of 64 scans and vendor provided software (OMNIC) was used to analyse the results, including the calculation of β-phase content. Differential scanning calorimetry (DSC) was used to investigate the crystalline phase of the polymer films on a TA Instruments DSC Q2000. The samples with an approximate weight of 2 mg, were heated at 10 ^oC/min from 0 to 250 ^oC under a 50 ml/min N_2 flow. The piezoelectric response of the samples was investigated by piezoresponse force microscopy (PFM) measurements using the MFP-3D™ AFM from Asylum Research (USA). A drive voltage of 3V (for sample S1), 5V (for sample S2) and 3V (for sample S4) was utilised for the measurements. Electrically conducting Pt/Ir-coated SCM-PIT probe with a resonance frequency of 100 kHz and a spring constant of 2.8 N/m were utilised for PFM imaging and further analysis carried out using vendor provided Igor Proanalysis software. The electrical measurements for the TENGs were carried out using a dynamic fatigue tester (Powil model YPS-1) in conjunction with a Tektronix MDO3022 oscilloscope and a Keysight B2981A picoammeter. The fatigue tester operates at various loads between 1-1000N and adjustable frequencies and allows for precise control over the impact load and frequencies.

3. Results and Discussions

3.1 Microstructure of ZnO nanosheets and ZnO-fluoropolymer composites

In literature, the hydrothermal/electrodeposition growth of ZnO, involving zinc nitrate hexahydrate and HMTA precursors, can be tuned to synthesise ZnO nanomaterials with various morphologies, including nanorods, nanobelts, nanoneedles etc. [23, 24]. The growth of all these ZnO nanostructures is known to follow a simple "nucleation and growth" procedure. During the nucleation step, the decomposition of the clusters of molecules results in particles that combine in a sequence to form a film on the surface of the substrate. This initial growth acts as a seed layer for the further growth and deposition of ZnO nanostructures and the processes are well understood to be dominated by the following equations [23, 25]:

$$½O_2 + H_2O + 2\,e^- \rightarrow 2OH^- \quad (1)$$

$$Zn^{2+} + 2OH^- \rightarrow Zn(OH)_2 \quad (2)$$

Now, for the growth of ZnO nanosheets using ED process, the presence of Al/Al_2O_3 substrates alongside HMTA and zinc precursor has been shown to be crucial [24]. It has been previously shown that the binding of $Al(OH)_4^-$ to the Zn^{2+} terminated surface is essential for suppressing the ZnO growth along the (0001) direction and promoting lateral growth of ZnO nanosheets [24]. The sources for hydroxide ions generated from the electrochemical method and the HMTA in the solution are consumed during the ZnO nanosheet growth through the following reactions:

$$(CH_2)_6N_4 + 6H_2O \rightarrow 6HCHO + 4NH_3 \quad (3)$$

$$NH_3 + H_2O \rightarrow NH_4^+ + OH^- \quad (4)$$

$$2OH^- + Zn^{2+} \rightarrow Zn(OH)_2 \quad (5)$$

$$Zn(OH)_2 \rightarrow ZnO_{(s)} + H_2O \quad (6)$$

$$Al^{3+} + OH^- \rightarrow Al(OH)_3 + OH^- \rightarrow AlO^-_2 \quad (7)$$

As Al is more active than Zn, it is oxidised to Al^{3+} and further forms AlO^-_2 in the electrolyte solution. This is followed by the absorption of AlO^-_2 by Zn^{2+} which slows down the growth of ZnO along (0002) orientation, resulting in a honeycomb-like network structure [18, 24] with a certain amount of Al elements included in the ZnO nanosheets (see Fig. 2). The ZnO nanostructures grown by this method on Si substrates (without Al) are typically nanorods with diameters varying from a few nanometres to tens of nanometres, depending on the experimental conditions of concentration, growth temperature etc. [24]. When an Al substrate is used, ZnO nanosheets are typically observed, which are particularly useful for the application in TENGs as the structure provides large surface areas for charge generation.

Moreover, due to morphologically inter-connected structure, as compared to the ZnO nanorods, the two-dimensional (2D) ZnO nanosheet structures are mechanically more stable under the large external mechanical loads [31]. The ZnO nanosheets on Al substrate grown for this work are shown in Fig. 2(a), with a preferred (0002) crystal orientation, perpendicular to the substrate. For a growth time of 3 hrs, the height of obtained ZnO nanosheets is ~5.2 μm (Fig. 2(b). Furthermore, the presence of Al in the ZnO nanosheets was confirmed by EDS measurement as shown in Fig. 2(a) inset.

Fig. 2 shows the surface and cross-sectional SEM images for the triboelectric negative portions of samples S2 and S4, comprising of (c, d) pristine PVDF and (e, f) $ZnSnO_3$-PVDF membranes deposited on top of the ZnO/Al substrates, respectively. It is evident from the SEM images that the respective dope solutions penetrate deep into the ZnO nanosheet architecture, and upon crystallisation during phase inversion process fill up the gaps in the structure to form uniform membranes. Upon the deposition of fluoropolymer membranes onto the ZnO/Al substrate, the overall thickness of the resulting structures is increased from ~5.2 μm to ~18.5 μm (Fig. 2(d)) and ~23.7 μm (Fig. 2(f)) for samples S1, S2 and S4, respectively. For both the PVDF/ZnO/Al and $ZnSnO_3$-PVDF/ZnO/Al samples, the surfaces exhibit high porosity, which is inherent to the phase inversion process. During the phase inversion process, the *N*, *N*-DMF solvent present in the dope solution escapes due to solvent anti-solvent interactions, leaving behind a high density of pores in the resulting membranes [16, 22]. Previous literature suggests that the charge density of the TENG can be enhanced by effectively controlling the microstructure and porosity of the polymer films [4, 9, 18, 26]. In fact, in a recent work carried out by Wang et al., nanostructured porous PVDF and PA6 membrane based TENG produced a significantly higher charge density (71 μCm^{-2}) than their smooth counterpart (48 μCm^{-2})[8]. The observed high porosity of phase-inversion membranes is highly beneficial in enhancing the performance of the TENGs owing to the increased effective surface area [1, 16] and will be discussed further in the following sections.

3.2 Electrical performance of TENGs

Fig. 3 shows the output open-circuit voltage (V_{OC}) and short-circuit current density (J_{SC}) of the assembled devices with variable forces ranging from 20 to 80 N (0.05-0.20 MPa). The TENG devices were measured at a fixed spacer distance of 8 mm and 5 Hz impact frequency. The output voltage of sample S1, consisting of ZnO nanosheets layer only, shows a modest

dependence on the applied force with a marginal, but inconsistent increase in the V_{OC} and J_{SC} values as observed in Fig. 3(a, b). In comparison, both the V_{OC} and J_{SC} values for the other three samples (S2, S3 and S4) increase almost linearly with the impact force. For instance, at a force of 80 N, the output voltage of sample S3 is ~310 V, which is consistent with the results of our previous work [15]; while the corresponding value of sample S4 is nearly twice at ~625 V. This increase in the output voltage is a combined effect of the addition of piezoelectric $ZnSnO_3$ nanoparticles in the PVDF host matrix as well as the piezoelectric/polarisation effect of interfacial ZnO nanosheets and will be discussed later in light of micro/nanoscale d_{33} measurements. For the samples incorporating $ZnSnO_3$, earlier studies, including ours, have indicated that stress induces polarisation and alignment effects, leading to generation of larger piezoelectric potential and higher charge density [16, 29, 30]. For the pristine PVDF/ZnO/Al system, the contact force still has a significant effect on the output performance of TENGs which is believed to arise from the elastic nature of the contacting materials, with a larger contact force substantially modifying the effective contact/charging area [21, 27, 28]. In fact, the slope of increase in the case of device S4 (7.55 V/N) is over twice that of device S3 (3.38 V/N) and nearly 2.5 times that of device S2 (2.98 V/N), showing the enhanced sensitivity of the device incorporating the interfacial ZnO nanosheet layer. The effect of embedding $ZnSnO_3$ in PVDF is significant in enhancing the output of TENG, especially at high force conditions, owing to the generation of larger piezoelectric potential and higher charge density from the PVDF-$ZnSnO_3$ system [16]. The output voltage and current density typically increase by 2.5 times for the PA6/($ZnSnO_3$-PVDF) TENG as compared to PA6/PVDF without $ZnSnO_3$ nanomaterial [16]. The current density for the devices S2 and S4 reaches ~10 mA/m^2 and ~40 mA/m^2, respectively, much larger than those (~1.25 mA/m^2 and ~3 mA/m^2) for PA6/PVDF TENG and PA6/($ZnSnO_3$-PVDF) TENGs reported in our previous work [16].

Device S1, consisting of Al/PA6 and ZnO/Al, has a relatively small electrical output, very different from other devices. When the electrical output of device S1 was measured without any spacer (see Fig. SI1, supplementary information), a marginal but consistent increase in the electrical output could be observed which arises from the generation of piezoelectric potential in the ZnO nanosheets. In the triboelectric configuration i.e. with a spacer, the high-density ZnO nanosheet structure should ideally provide substantially large effective contact area due to the nanostructures. Moreover, as the polymeric PA6 membrane has an elastic nature and ZnO nanosheet layer has high surface area, high density of

triboelectric charges is expected to be generated, which should increase with increasing force due to the increased contact surface area. However, as observed in Fig. 3(a), the output performance of S1 shows almost no appreciable change with impact force with a rather poor sensitivity value of 0.1 V/N. Compared to Al, PA6 is more triboelectric positive, and upon contact between the two surfaces, triboelectric potential should be generated owing to the different inherent electronic affinities of the two materials. However, the bottom Al electrode cannot directly contact the PA6 due to the presence of an interfacial ZnO nanosheet layer. The contact between PA6 and ZnO nanosheets will induce negative triboelectric charges as PA6 is more positive in the triboelectric series table. However, the mechanical deformation of ZnO nanosheets under contact will generate a piezoelectric potential concurrently inside the nanosheets, and piezoelectric charges. As such, the electrical output of sample S1 is a combined effect of piezoelectric and triboelectric effects.

Now, considering devices S3 and S4, the only difference between them is the incorporation of ZnO nanosheets at bottom of the $ZnSnO_3$-PVDF composite film for device S4. On their own, the ZnO/Al system is only able to provide a small voltage and current output of ~20 V and ~1 mA/m^2, respectively; however, working synergistically with the $ZnSnO_3$-PVDF composite film, the huge increase in output performance for S4 is considered to be caused mainly by the polarisation induced charges by the piezoelectric ZnO nanosheets. The pressure induced polarisation effects in the $ZnSnO_3$-PVDF inorganic-organic composite and the inherent piezoelectric, ferroelectric nature of the ZnO component, the electric dipoles inside the composite membrane and ZnO nanosheets will be oriented to enhance the surface charge density of the contact interface [29, 30]. This preferred polarisation growth direction of dipoles caused due to the interfacial dipole-dipole interaction was further imaged using piezoelectric force microscopy and is discussed in the next section. The influence of ZnO nanosheets to the performance of the TENG devices can be clearly seen by comparing S3 and S4 devices at various forces, especially in the remarkable increase in the current density. Within the force range tested, both the V_{OC} and J_{SC} of S4 increase more significantly compared to those of S3, with the slope of S4 (7.55 V/N) more than double of S3 (3.38 V/N), implying the significant effect of ZnO nanosheets on TENG performance (see Table 2, summary of the output performance of all the devices). The sensitivity values for device S4 are very similar to those reported earlier by Chen et al., for the poly(vinylidenefluoride-co-trifluoroethylene) (P(VDF-TrFE)) and PDMS based TENG [31]. It is understood that during the initial stage of measurement of TENGs i.e. before the contact of the two triboelectric

layers, neither piezoelectric no triboelectric potential exists between the two surfaces. When an external vertical force is applied to the top PA6/Al layer and it touches the bottom triboelectric negative surface ($ZnSnO_3$-PVDF/ZnO/Al), the physical contact between the surfaces results in a charge transfer between the PA6 and PVDF. Since PVDF tends to gain electrons, the negative charges are transferred to PVDF, while PA6 acquires positive triboelectric charges. When the applied force is raised further, the introduction of stress onto the $ZnSnO_3$ nanocubes and indeed the ZnO nanosheets leads to the creation of a strong and cumulative piezoelectric potential. When the applied force is released, the structure starts to bounce back, leading to the movement/flow of charges through the external circuit. Thus, the incorporation of an interfacial layer induces a high density of polarisation charges through piezoelectric nanomaterials in the PVDF matrix.

The output performance of all the assembled devices was also tested as a function of operating frequency between 1–9 Hz, at a fixed force of 50 N and spacer distance of 8 mm (Fig. 4). As the impact frequency is increased from 1 to 9 Hz, the output voltage for sample S1 increases from ~10 to 30 V, the corresponding current density from ~0.9 to ~4 mA/m^2 with a maximum charge density per pulse of 16.89 $\mu C/m^2$. Correspondingly for sample S2, V_{OC} increases from ~20 to ~140 V, J_{SC} from 1 to 4 mA/m^2 and a maximum charge density per pulse of 68.41 $\mu C/m^2$. To best elucidate the advantage of utilizing the interfacial ZnO nanosheet layer, the outputs of device S3 and S4 at different frequencies are shown in Fig. 4(g, h). In the used frequency range, the output voltage of S3 increases from ~50 to ~ 280 V, the current density from 2.5 to 15 mA/m^2 with a corresponding maximum charge density of 77.45 $\mu C/m^2$. For device S4, the increase in output is significantly higher, with V_{OC} increasing from ~70 to ~ 310 V, Jsc from 2.5 to 25 mA/m^2 and a maximum charge density per pulse of 100.66 $\mu C/m^2$, further indicating the existence of ZnO nanosheets, through polarization-induced charges, has a significant effect on the TENG output. From Fig. 4, it can also be observed that for nearly all the samples, an increase in the operating frequency from 7 Hz to 9 Hz does not significantly alter the output, indicating an ideal working frequency of about 7 Hz. Thus, the developed TENG structures are highly suitable for harvesting low-frequency vibration and impact conditions.

Fig. 5 displays the output power density (calculated by $W=I_{peak}^2R/A$, here A the device area) measurements as a function of load resistance from 1-1000 MΩ, for devices S3 and S4. It can be observed that the maximum power density is delivered at a load resistance of ~30 and ~40 MΩ for S3 and S4, respectively. At a constant force of 50 N, a maximum peak

power density of ~1.8 W/m^2 is achieved for S4, while that for S3 is ~0.11 W/m^2, further clearly indicating that ZnO nanosheet layer plays a major role in device performance. The instantaneous power being delivered by a 4 cm^2 TENG (S4) was further used to power 35 red LEDs mounted on a PCB board. When the TENG was driven by a 50 N force at 5 Hz without any charge storage, it could lighten the LEDs, but with relatively weak light intensity. The full brightness of the LEDs could be achieved by using a 1 μF storage capacitor which was charged up by repeated pressing of the TENG for about 50 times, as shown in Fig. 6(a). Fig. 6(b) shows the stability of the output voltage for sample S4 as a function of impact cycles. The stability tests were carried out at a fixed condition of 5 Hz impact frequency and a force of 30 N. The measured output voltage does not attenuate, but increases slowly from ~260 to ~300 V during the 9000 cyclic tests. This phenomenon is quite different from that being reported by most other researchers, wherein the output voltage decreases with the increase in the number of cyclic tests [15]. The observed increase in our case may be attributed to the surface deformation caused by the prolonged impact which allows more and more vacant space between ZnO nanosheets to be filled during cyclic impact, allowing more polarisation induced charges to contribute to the triboelectric effect.

3.3 Mechanism for performance enhancement of TENGs

Though a variety of factors can potentially influence the electrical output of the TENG devices, considering the consistency of the experimental parameters, including device dimensions, testing protocol and fluoropolymer membrane deposition conditions; the significant difference observed in the electrical outputs of sample S3 and S4 most likely originates from the variation of the surface charge density and coupling of the piezoelectric and triboelectric effects. Fig. 7 shows the generation mechanism plots of piezoelectric, triboelectric and combined effect in generating the V_{OC} during press and release cycle. Both the pristine PVDF and $ZnSnO_3$-PVDF membranes synthesised *via* phase-inversion method were found to have high β-phase content of ~61% and 72%, respectively which is consistent with the results of our previous works [11, 16]. The high β-phase contributes to the increase in piezoelectric coefficient of the membranes [11], which contributes to the high piezoelectric constants observed for the samples. We have investigated the material properties of the PVDF, $ZnSnO_3$-PVDF and $ZnSnO_3$-PVDF/ZnO nanosheets using FTIR and DSC measurements with the results shown in the supplementary information (Fig. SI2). The DSC measurements for PVDF and 5wt% $ZnSnO_3$-PVDF membranes revealed crystallinity values

of about 36% and 47%, respectively. The observed increase in the crystallinity and the β-phase content upon the addition of $ZnSnO_3$ is consistent with our previous work and arises due to the interfacial interactions between PVDF and $ZnSnO_3$ nanomaterial [16]. Thus, it seems that the underlying ZnO nanosheet structure has no significant effect on the phase-inversion process and the ensuing crystallinity and β-phase content of the fluoropolymer films. The marginal (~10%) increase of the β-phase and crystallinity values cannot fully explain the significant increase in the power output of the TENGs. In fact, all the electrical characterisation data indicates that the incorporation of interfacial ZnO nanosheet layer has a more profound effect on the output performance of the TENGs, possibly through polarisation induced charges [10, 32, 33]. To understand the underlying mechanism responsible for this significant increase in the performance, piezoelectric measurements of the samples were carried out.

PFM analysis was used to measure the piezoelectric coefficient and indicative polarisation direction for the samples. Fig. 8 shows the PFM amplitude and phase for the pristine ZnO nanosheets, PVDF/ZnO and $ZnSnO_3$-PVDF/ZnO samples used for devices S1, S2 and S4 respectively. The piezoelectric characteristics of sample S3 can be found in our earlier work [16]. The amplitude of the piezoelectric signal is related to the piezoelectric coefficient (electromechanical coupling) of the samples, while the phase of the signal reflects the polarisation direction or the orientation of the domains. From the PFM amplitude images, it can be observed that the amplitude displayed by S4 has much higher contrast than those of sample S1 & S2, while sample S1 and S2 exhibit a much broader distribution of domains. Now, the PFM signal is given by

$$A = d_{33} V_{ac} Q \tag{8}$$

where d_{33} is the piezoelectric strain coefficient, V_{ac} is the driving voltage, and Q is the quality factor [34]. The obtained piezoelectric coefficient of -41 pmV^{-1} for sample S1 comprising of pristine ZnO nanosheets layer is comparable to the values reported in the literature for the same type of materials [27] and is higher than that for bulk ZnO [27]. The large d_{33} for sample S1 is attributed to nanoscale dimensions of the (0002) oriented ZnO nanosheets [26, 35]. Similarly, the measured d_{33} values for S2 and S4 are -50 pmV^{-1} and -74 pmV^{-1}, respectively, and show a marked improvement as compared to our previous work [16]. This improved piezoelectric effect clearly notifies the observed enhancement in triboelectric output voltage V_{OC} of S4 as compared to S1 and S2. Moreover, the PFM phase image obtained for sample S4 clearly shows a preferential polarisation growth direction of dipoles

(see the white dot highlighted area in Fig. 8(f)). This significantly enhanced domain size and piezoelectric response for S4 are attributed to the interfacial dipole-dipole interaction with the ferroelectric polarization of PVDF, which promotes the alignment with the polar axis of ZnO nanosheets. It has been reported that upon the application of force to ZnO nanosheets, they tend to buckle and generate piezoelectric potential by inducing a positive potential on the stretched side and a negative potential at the compressed side as shown in Fig. 1 [32]. This assists further in the injection of charges by the interfacial piezoelectric ZnO nanosheet layer between the contact surfaces [33]. When the spin coated PVDF, $ZnSnO_3$-PVDF dope solution deposited on the ZnO nanosheet layer undergoes fast quenching at low temperature, a strong thermal field gradient is induced, which can also cause the crystals to align along the thermal field direction [22]. Also, the thermal stress after fast quenching, arising from the difference in thermal expansion coefficients between $ZnSnO_3$-PVDF dope solution and interfacial ZnO layer is expected to give tensile stress which can reorient the dipoles in preferential direction. Furthermore, the O–H groups of the water molecules can form hydrogen bonds with the C–F groups of PVDF, leading to their spatial orientation. During the solvent, anti-solvent interactions, the mass exchange between the solvent and non-solvent is so fast that the liquid–liquid demixing takes places almost immediately, resulting in enhanced polymer concentration near the interfacial region [22]. This increase in the polymer concentration leads to better packing of the CH_2-CF_2 dipoles, leading to the formation of β-phase [34]. At low quenching temperatures, the crystallisation beginning from the surface and proceeding towards the inside of the film is slow [22]. As water is a dipolar molecule, the electric field acts on the initial surface, inducing aligned β-crystals, which in turn causes the alignment of the β-phase crystals in the sequential crystallisation. Using first-principle calculations, Bystrov et al. have shown that the interaction between PVDF molecular chains leads to the orientation of each molecular dipole moment along one direction parallel to the chain plane [36]. On the other hand, the molecular interaction in PVDF will lead to the same orientation direction as ZnO growth direction [22], thus they increase the charge density more profoundly, hence increasing the overall efficiency of TENG devices.

4 Conclusion

In summary, we have reported on the technique to fabricate high-performance TENGs by incorporating an interfacial piezoelectric ZnO nanosheet layer underneath the triboelectric negative fluoropolymer membranes. The enhancement in performance of the TENG

is significant, with V_{OC} and J_{SC} values increasing from 310 V and 10 mA/m^2 (charge density of 77.45 μCm^{-2}) to ~625 V and 40 mA/m^2 (charge density of 100.66 μCm^{-2}), and has been attributed to stress-induced polarisation effect from the $ZnSnO_3$-PVDF/ZnO structure. The well-aligned ZnO nanosheets not only enhance the effective surface area, but also lead to preferential polarisation growth direction of dipoles, further improving the piezoelectric coefficient up to -74 pm V^{-1}. This enhancement assists in charge injection by piezoelectric interlayer on to the surface of $ZnSnO_3$-PVDF membrane, improving the charge density to ~100.66 μC/m^2 from a value of 77.45 μC/m^2 (without interfacial ZnO nanosheet layer), which in-turn tremendously improves the power density from 0.11 to ~1.8 W/m^2. The facile synthesis of ZnO nanostructures alongside the simple phase inversion technique provides an easy route to couple piezoelectric and triboelectric mechanisms to yield high-performance TENG devices, which could be an excellent candidate for self-powered electronic systems.

Acknowledgements

Materials support from Solvay Speciality Polymers and William Blythe Ltd. (United Kingdom) is greatly acknowledged.

References

[1] Z. L. Wang, L. Lin, J. Chen, S. Niu, and Y. Zi, *Triboelectric Nanogenerators*. Cham: Springer International Publishing, 2016.

[2] Z. L. Wang, *Nanogenerators for Self-powered Devices and Systems*. 2005.

[3] Z. L. Wang and J. Song, "Piezoelectric Nanogenerators Based on Zinc Oxide Nanowire Arrays," *Science (80-.).*, vol. 312, no. 5771, pp. 242–246, 2006.

[4] F. R. Fan, Z. Q. Tian, and Z. Lin Wang, "Flexible triboelectric generator," *Nano Energy*, vol. 1, no. 2, pp. 328–334, 2012.

[5] Z. Lin, J. Chen, and J. Yang, "Recent progress in triboelectric nanogenerators as a renewable and sustainable power source," vol. 2016, 2016.

[6] X. Yang and W. A. Daoud, "Triboelectric and Piezoelectric Effects in a Combined Tribo-Piezoelectric Nanogenerator Based on an Interfacial ZnO Nanostructure," *Adv. Funct. Mater.*, vol. 26, no. 45, pp. 8194–8201, 2016.

[7] M. Choi, G. Murillo, S. Hwang, J. W. Kim, J. H. Jung, C.-Y. Chen, and M. Lee, "Mechanical and Electrical Characterization of PVDF-ZnO Hybrid Structure for Application to Nanogenerator," *Nano Energy*, vol. 33, no. February, p. , 2017.

[8] H. Y. Li, L. Su, S. Y. Kuang, C. F. Pan, G. Zhu, and Z. L. Wang, "Significant Enhancement of Triboelectric Charge Density by Fluorinated Surface Modification in Nanoscale for Converting Mechanical Energy," *Adv. Funct. Mater.*, vol. 25, no. 35, pp. 5691–5697, 2015.

[9] X. S. Zhang, M. Di Han, R. X. Wang, F. Y. Zhu, Z. H. Li, W. Wang, and H. X. Zhang,

"Frequency-multiplication high-output triboelectric nanogenerator for sustainably powering biomedical microsystems," *Nano Lett.*, vol. 13, no. 3, pp. 1168–1172, 2013.

[10] F. R. Fan, W. Tang, and Z. L. Wang, "Flexible Nanogenerators for Energy Harvesting and Self-Powered Electronics," *Adv. Mater.*, vol. 28, no. 22, pp. 4283–4305, 2016.

[11] H. Kim, S. M. Kim, H. Son, H. Kim, B. Park, J. Ku, J. I. Sohn, K. Im, J. E. Jang, J.-J. Park, O. Kim, S. Cha, and Y. J. Park, "Enhancement of piezoelectricity via electrostatic effects on a textile platform," *Energy Environ. Sci.*, vol. 5, no. 10, p. 8932, 2012.

[12] W.-S. Jung, M.-G. Kang, H. G. Moon, S.-H. Baek, S.-J. Yoon, Z.-L. Wang, S.-W. Kim, and C.-Y. Kang, "High output piezo/triboelectric hybrid generator.," *Sci. Rep.*, vol. 5, p. 9309, 2015.

[13] M. Han, X. Zhang, B. Meng, W. Liu, W. Tang, X. Sun, and W. Wang, "r - Shaped Hybrid Nanogenerator with Enhanced Piezoelectricity," no. 10, pp. 8554–8560, 2013.

[14] X. Li, Z. H. Lin, G. Cheng, X. Wen, Y. Liu, S. Niu, and Z. L. Wang, "3D fiber-based hybrid nanogenerator for energy harvesting and as a self-powered pressure sensor," *ACS Nano*, vol. 8, no. 10, pp. 10674–10681, 2014.

[15] X. Chen, M. Han, H. Chen, X. Cheng, Y. Song, Z. Su, Y. Jiang, and H. Zhang, "A wave-shaped hybrid piezoelectric and triboelectric nanogenerator based on P(VDF-TrFE) nanofibers," *Nanoscale*, vol. 9, no. 3, pp. 1263–1270, 2017.

[16] N. Soin, P. Zhao, K. Prashanthi, J. Chen, P. Ding, E. Zhou, T. Shah, S. C. Ray, C. Tsonos, T. Thundat, E. Siores, and J. Luo, "High performance triboelectric nanogenerators based on phase-inversion piezoelectric membranes of poly(vinylidene fluoride)-zinc stannate (PVDF-ZnSnO3) and polyamide-6 (PA6)," *Nano Energy*, vol. 30, no. October, pp. 470–480, 2016.

[17] Y. Liu, Y. Sun, F. Zeng, J. Liu, and J. Ge, "Effect of POSS nanofiller on structure, thermal and mechanical properties of PVDF matrix," *J. Nanoparticle Res.*, vol. 15, no. 12, pp. 1–10, 2013.

[18] H. Huang, H. Wang, B. Li, X. Mo, H. Long, Y. Li, H. Zhang, D. L. Carroll, and G. Fang, "Seedless synthesis of layered ZnO nanowall networks on Al substrate for white light electroluminescence," *Nanotechnology*, vol. 24, no. 31, p. 315203, 2013.

[19] M. H. Zhao, Z. L. Wang, and S. X. Mao, "Piezoelectric characterization individual zinc oxide nanobelt probed by piezoresponse force microscope," *Nano Lett.*, vol. 4, no. 4, pp. 587–590, 2004.

[20] Z. L. Wang, G. Zhu, Y. Yang, S. Wang, and C. Pan, "Progress in nanogenerators for portable electronics," *Mater. Today*, vol. 15, no. 12, pp. 532–543, 2012.

[21] M. Taghavi and L. Beccai, "A contact-key triboelectric nanogenerator: Theoretical and experimental study on motion speed influence," *Nano Energy*, vol. 18, pp. 283–292, 2015.

[22] N. Soin, D. Boyer, K. Prashanthi, S. Sharma, A. A. Narasimulu, J. Luo, T. H. Shah, E. Siores, and T. Thundat, "Exclusive self-aligned β-phase PVDF films with abnormal piezoelectric coefficient prepared via phase inversion," *Chem. Commun.*, vol. 2, no. 39, pp. 1–4, 2015.

[23] M. Kumar and C. Sasikumar, "Electrodeposition of Nanostructured ZnO Thin Film: A Review," *Am. J. Mater. Sci. Eng.*, vol. 2, no. 2, pp. 18–23, 2014.

[24] K. O. Iwu, V. Strano, A. Di Mauro, G. Impellizzeri, and S. Mirabella, "Enhanced Quality, Growth Kinetics, and Photocatalysis of ZnO Nanowalls Prepared by Chemical Bath Deposition," *Cryst. Growth Des.*, vol. 15, no. 9, pp. 4206–4212, 2015.

[25] S. Moeinzadeh and E. Jabbari, *Handbook of Nanomaterials Properties*, no. April. 2014.

[26] M. Ghosh and M. G. Rao, "Growth mechanism of ZnO nanostructures for ultra-high piezoelectric d33 coefficient," *Mater. Express*, vol. 3, no. 4, pp. 319–327, 2013.

[27] Z. L. Wang, "Triboelectric nanogenerators as new energy technology and self-powered sensors - Principles, problems and perspectives.," *R. Soc. Chem.*, vol. 0, no. 11, pp. 1–12, 2014.

[28] S. Niu, S. Wang, L. Lin, Y. Liu, Y. S. Zhou, Y. Hu, and Z. L. Wang, “Theoretical study of contact-mode triboelectric nanogenerators as an effective power source,” *Energy Environ. Sci.*, vol. 6, no. 12, p. 3576, 2013.

[29] G. Wang, Y. Xi, H. Xuan, R. Liu, X. Chen, and L. Cheng, “Hybrid nanogenerators based on triboelectrification of a dielectric composite made of lead-free ZnSnO3 nanocubes,” *Nano Energy*, vol. 18, pp. 28–36, 2015.

[30] K. Y. Lee, D. Kim, J. H. Lee, T. Y. Kim, M. K. Gupta, and S. W. Kim, “Unidirectional high-power generation via stress-induced dipole alignment from ZnSnO3 nanocubes/polymer hybrid piezoelectric nanogenerator,” *Adv. Funct. Mater.*, vol. 24, no. 1, pp. 37–43, 2014.

[31] X. Chen, Y. Song, Z. Su, H. Chen, X. Cheng, J. Zhang, M. Han, and H. Zhang. "Flexible fiber-based hybrid nanogenerator for biomechanical energy harvesting and physiological monitoring." *Nano Energy*, vol. 38, pp. 43-50, 2017.

[32] K.-H. Kim, B. Kumar, K. Y. Lee, H.-K. Park, J.-H. Lee, H. H. Lee, H. Jun, D. Lee, and S.-W. Kim, “Piezoelectric two-dimensional nanosheet/anionic layer heterojunction for efficient direct current power generation.,” *Sci. Rep.*, vol. 3, p. 2017, 2013.

[33] X. Yang and W. A. Daoud, “Triboelectric and Piezoelectric Effects in a Combined Tribo-Piezoelectric Nanogenerator Based on an Interfacial ZnO Nanostructure,” *Adv. Funct. Mater.*, 2016.

[34] K. Prashanthi, H. Zhang, V. Ramgopal Rao, and T. Thundat, “Local piezoelectric response of ZnO nanoparticles embedded in a photosensitive polymer.” *Phys. Status Solidi RRL*, vol. 6, no. 2, pp. 77-79, 2012.

[35] M. Zhang, A. Q. Zhang, B. K. Zhu, C. H. Du and Y. Y. Xu, *J. Membr. Sci.*, 2008, 319, 169.

[36] V. S. Bystrov, N. K. Bystrova, E. V. Paramonova, G. Vizdrik, A. V.Sapronova, M. Kuehn, H. Kliem and A. L. Kholkin, *J. Phys.: Condens. Matter*, 2007, 19, 456210.

Table 1: Summary of sturtcutres of the fabricated TENG devices.

Sample	Top layer	Bottom layer	Device structure
S1	Al/PA6	ZnO/Al	(Al/PA6)/(ZnO/Al)
S2	Al/PA6	PVDF/ZnO/Al	(Al/PA6)/(PVDF/ZnO/Al)
S3 (without interfacial ZnO layer)	Al/PA6	5wt%$ZnSnO_3$-PVDF/Al	(Al/PA6)/($ZnSnO_3$-PVDF/Al)
S4 (with interfacial ZnO layer)	Al/PA6	5wt%$ZnSnO_3$-PVDF/ZnO/Al	(Al/PA6)/($ZnSnO_3$-PVDF/ZnO/Al)

Table 2: Summary of the output characteristics of the fabricated TENG devices.

Device	Voc (V)	Jsc (mAm^{-2})	Charge density (μCm^{-2})	d_{33} (pmV^{-1})	Sensitivity (V/N)
S1	40	3	16.9	-41	0.1
S2	280	8	68.4	-50	2.98
S3	310	10	77.5	-54*	3.38
S4	625	40	100.6	-74	7.55

*- measured value reported in our earlier work [16].

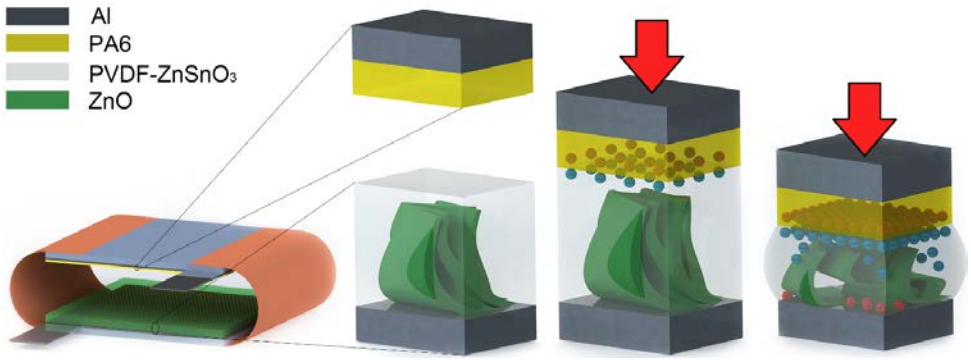

Fig. 1. Schematic and working mechanism of the TENG with an incorporated interfacial ZnO nanosheet layer. The red arrow describes the application of force, leading to the generation of triboelectric potential, and piezoelectric potential in the ZnO nanosheets by inducing a positive potential (red spheres) on the stretched side and a negative potential (blue spheres) at the compressed side.

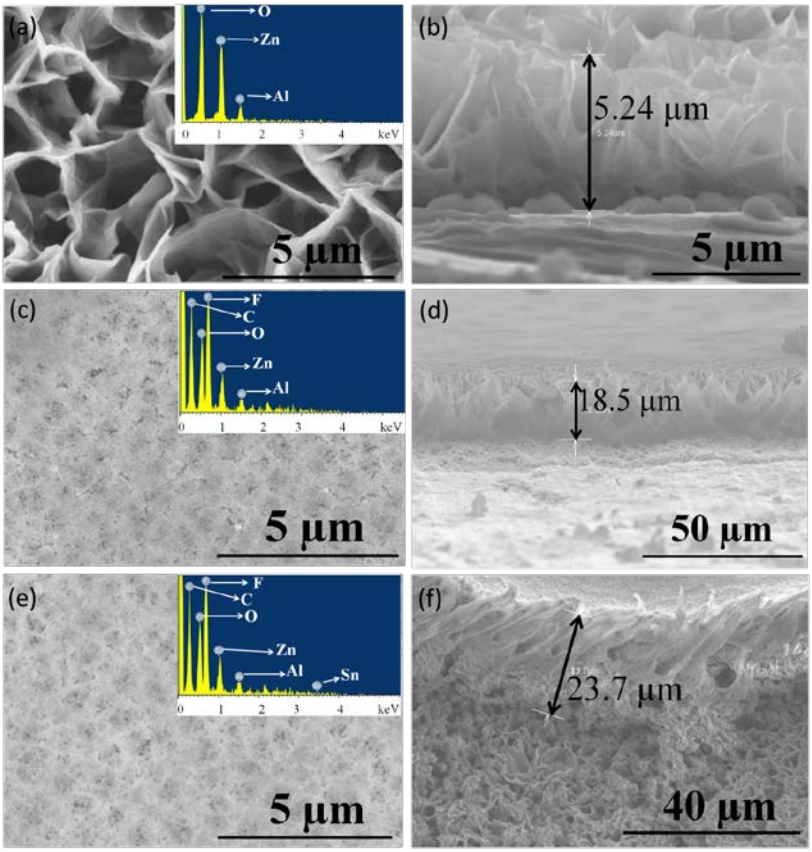

Fig. 2. SEM top view image (a) and cross-sectional view image (b) for the pristine ZnO nanosheets on Al substrate, (c) and (d) for PVDF membrane on ZnO/Al, (e) and (f) for $ZnSnO_3$/PVDF membrane on ZnO/Al device, respectively. The insets in (c) and (e) are the EDS measurement results for the corresponding samples.

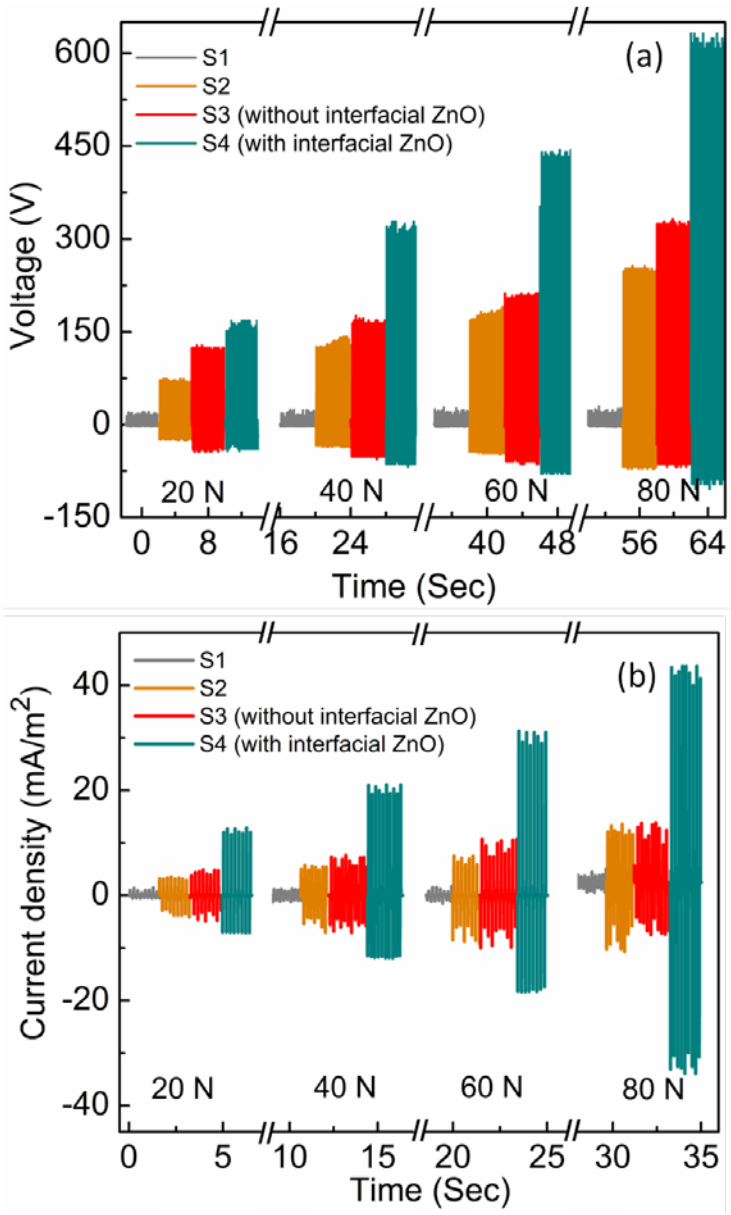

Fig. 3. (a) Open circuit voltage (V_{OC}) and (b) short circuit current density (J_{SC}) for TENGs being operated at various impact forces (at a constant 5 Hz working frequency).

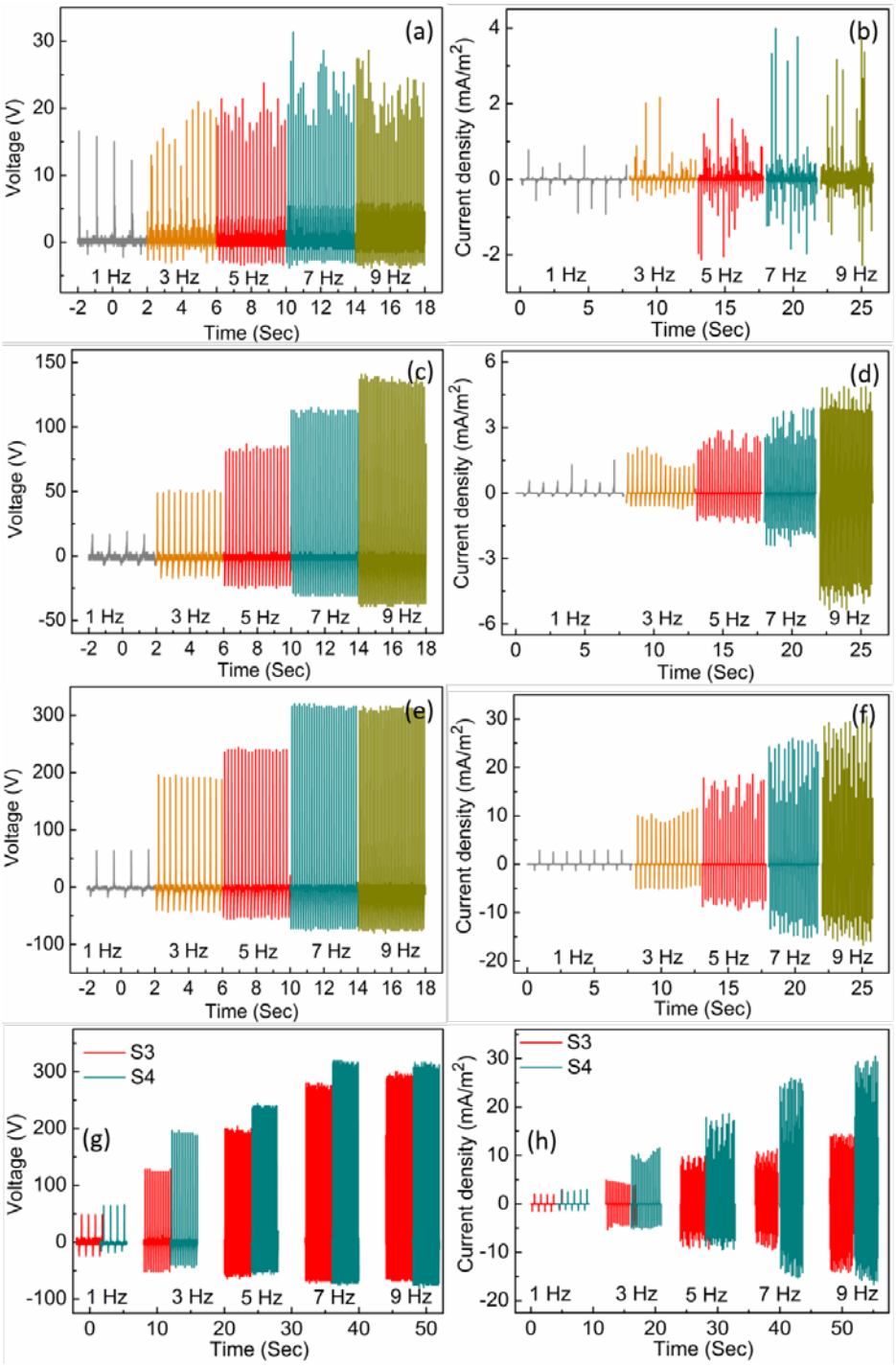

Fig. 4. (a) Open circuit voltage (Voc) and (b) short circuit current densities (J_{SC}) of sample S1, corresponding Voc and Jsc values (c) and (d) for sample S2, while (e) and (f) show the Voc and Jsc values for sample S4. The effect of an interfacial ZnO nanosheet layer is best illustrated in the variation of (g) Voc and (h) Jsc values for samples S3 and S4. All measurements were carried out at a constant force of 50 N and spacer distance of 8 mm.

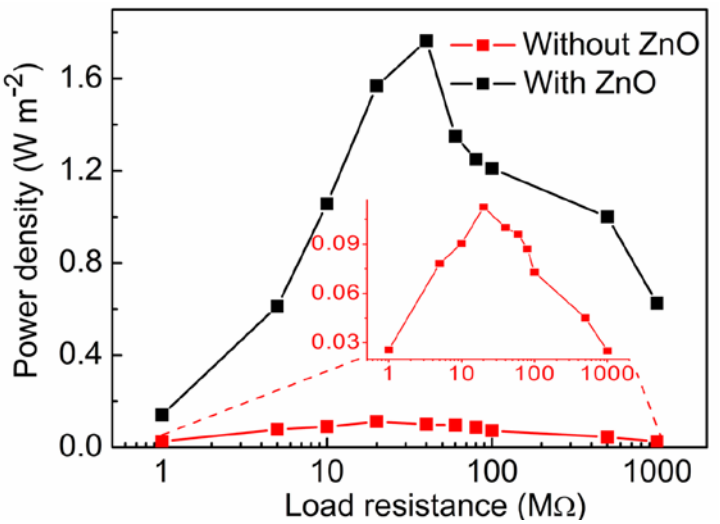

Fig. 5. Comparison of output power density vs. load, showing the maximum power outputs for samples S3 and S4 at ~30 and ~40 MΩ, respectively. The inset shows the blow-up of the power vs. load curve for sample S3.

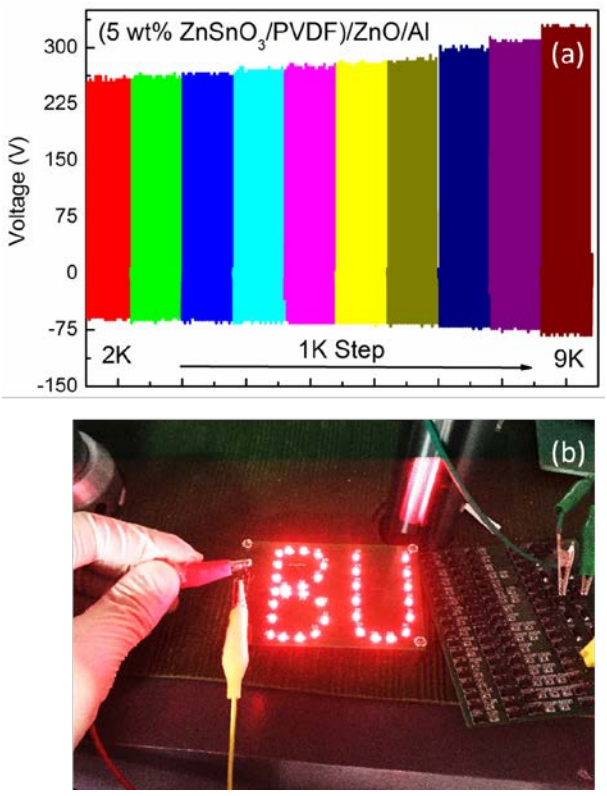

Fig. 6. (a) The stability test of TENG sample S4 carried out for 9000 cycles at a force of 30 N at a driving frequency of 5 Hz, (b) lighting a group of 35 red LED's with as fabricated TENG device by charging a 1 μF capacitor.

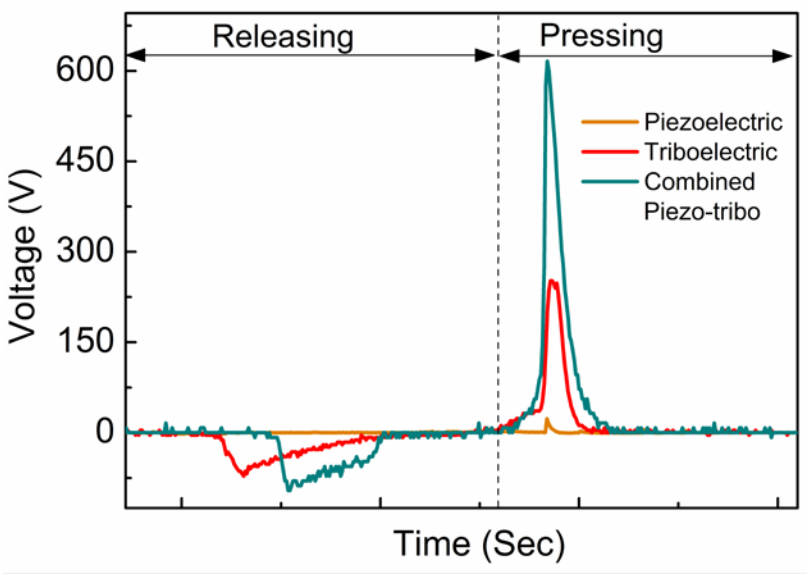

Fig. 7. A graph of the piezo/triboelectric output voltages simultaneously measured in a single press-and-release cycle.

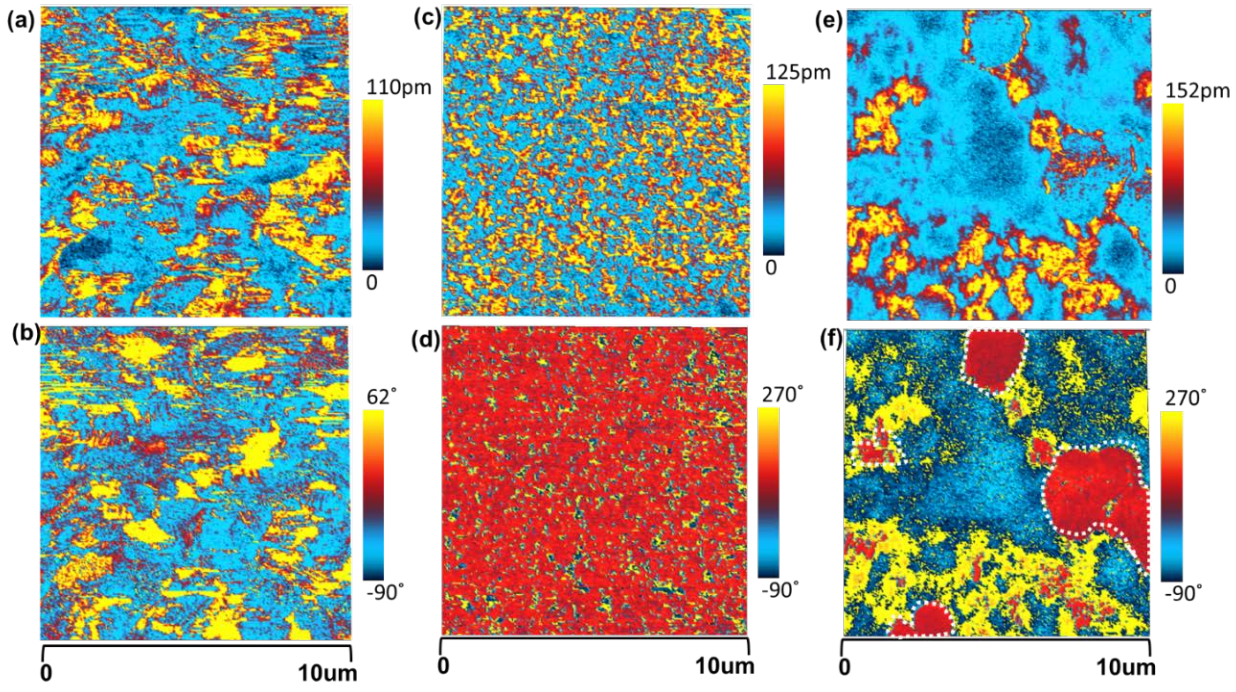

Fig. 8: (a) PFM amplitude image and (b) PFM phase for S1, (c) and (d) for S2, (e) and (f) for S4 devices, respectively. White dot highlighted areas in (f) show preferential growth of polarisation.